

Article

Global Energy Production Computation of a Solar-Powered Smart Home Automation System Using Reliability-Oriented Metrics

Raul Rotar ^{*}, Sorin Liviu Jurj , Robert Susany, Flavius Opritoiu and Mircea Vladutiu

Department of Computers and Information Technology, Politehnica University of Timisoara, 2 V. Parvan Blvd, 300223 Timisoara, Romania; jurjsorinliviu@yahoo.de (S.L.J.); robert.susany@student.upt.ro (R.S.); flavius.opritoiu@cs.upt.ro (F.O.); mircea.vladutiu@cs.upt.ro (M.V.)

* Correspondence: raul.rotar@student.upt.ro

Abstract: This paper presents a modified global energy production computation formula that replaces the traditional Performance Ratio (PR) with a novel Solar Reliability Factor (SRF) for mobile solar tracking systems. The SRF parameter describes the reliability and availability of a dual-axis solar tracker, which powers a smart home automation system entirely by using clean energy. By applying the SRF in the global energy production formula of solar tracking systems, we can predict the energy generation in real time, allowing proper energy management of the entire smart home automation system. Regarding static deployed Photovoltaic (PV) systems, the PR factor is preserved to compute the power generation of these devices accurately. Experimental results show that the energy production computation constantly fluctuates over several days due to the SRF parameter variation, showing a 26.11% reduction when the dual-axis solar tracker's availability is affected by system errors and maximum power generation when the solar tracking device is operating in optimal conditions.

Keywords: solar reliability factor; solar tracker; smart home automation system; fault coverage; hybrid testing; global energy production



Citation: Rotar, R.; Jurj, S.L.; Susany, R.; Opritoiu, F.; Vladutiu, M. Global Energy Production Computation of a Solar-Powered Smart Home Automation System Using Reliability-Oriented Metrics. *Energies* **2021**, *14*, 2541. <https://doi.org/10.3390/en14092541>

Academic Editors: Mariusz Filipowicz and Krzysztof Sornek

Received: 31 March 2021
Accepted: 26 April 2021
Published: 28 April 2021

Publisher's Note: MDPI stays neutral with regard to jurisdictional claims in published maps and institutional affiliations.



Copyright: © 2021 by the authors. Licensee MDPI, Basel, Switzerland. This article is an open access article distributed under the terms and conditions of the Creative Commons Attribution (CC BY) license (<https://creativecommons.org/licenses/by/4.0/>).

1. Introduction

This section presents insight regarding new perspectives on computing the global energy production of mobile PV systems by substituting the Performance Ratio (PR) factor with a novel Solar Reliability Factor (SRF) parameter, as well as a detailed overview of solar-powered smart home automation systems.

1.1. The Performance Ratio of Static and Mobile PV Systems

Due to recent advancements in the Internet of Things (IoT) domain, a plethora of smart electronic devices have been implemented in different domains, improving the quality of life for many people around the world [1], with a report from Statista forecasting that the IoT's global market share will reach 1.6 trillion U.S. dollars by 2025 [2]. This demonstrates the importance of IoT in the future of communication between humans and smart objects. These smart objects (e.g., smart sensors, actuators, and cameras) are often found in automation systems such as security and home automation systems. Regarding smart home automation systems, their main advantages compared to other automated systems are the comfort and flexibility given by remote features such as switching the lights, voice control, and monitoring security cameras in real time. The sensor's energy management is an essential aspect of smart home automation systems due to their constant energy consumption specifications and dependability on the power grid [3]. When considering the recent efforts made by many countries towards the goal of replacing carbon-based emissions with renewable energy sources by the year 2050 [4], the need for using clean

energy sources for powering smart home automation systems is of significant importance for lowering the cost of energy consumption and for a sustainable future.

The most efficient clean energy collectors are considered to be the dual-axis solar tracking systems, which can gather the maximum amount of solar energy when compared to their static counterparts due to their mobility on both the horizontal and vertical axis. One of the quality indicators for a durable and robust solar tracking device is given by the PV panel's energy production. The energy management can be directly linked to the energy production of energy-harvesting devices such as fixed-tilted PV panels, solar concentrators, and solar trackers, to name only a few. The energy production estimation can be computed with the help of a variety of parameters such as the total surface area and the yield of a PV panel [5], solar radiation [6], and Performance Ratio (*PR*) factor [7].

However, regarding solar tracking devices, the parameters mentioned above for calculating the energy production are not sufficient since the electrical equipment of a mobile solar tracking device can be affected by hardware, software, and in-circuit errors [8], which can alter its long-term performance and durability. Regarding this aspect, in this paper we make use of a set of reliability metrics to calculate the Solar Reliability Factor (*SRF*) parameter of a solar tracking device that will be further used in a solar-powered smart home automation system's energy production global formula.

The reliability-oriented metrics make use of a precomputed Solar Test Factor (*STF*), which targets quantifying the fault coverage using data from various test scenarios (software, hardware, and in-circuit testing (*ICT*)). The experimental data are collected over two weeks with the help of testing equipment coupled to the dual-axis solar tracking system. The *SRF* parameter will be only used to calculate the power generation of mobile PV systems equipped with dual-axis solar tracking devices. Simultaneously, the traditional *PR* factor will be preserved for computing the energy production of static deployed PV systems. A comparison between the *SRF* parameter and the *PR* factor is also provided in this paper to demonstrate the validity of the reliability-oriented metrics.

1.2. Solar-Powered Internet of Things (IoT)-Based Smart Home Automation Systems

Current advancements in the IoT domain show a growing interest in developing solar-powered smart home automation systems [9–15], as well as employing reliable and efficient energy production formulas, which are used to optimize the energy management of future smart green homes.

Sustainable home automation with advanced security features and powered entirely by green energy has become a feasible solution for today's social standards. The authors in [9] propose IoT-based smart home automation equipped with sensors for motion, fire, and gas leak detection. Their smart home design makes use of an Arduino mini and Node Microcontroller Unit (MCU) for monitoring the entire solar-powered sensor network. Additionally, the employed equipment can be controlled via Wi-Fi capabilities with a phone application such as Blynk or Alexa. Similarly, the authors in [10] propose a solar-assisted advanced smart home automation that integrates a solar module, composed of a PV array, DC-DC converter, Battery Charge Controller, and Battery Bank, which is tethered to the home automation module comprising a mobile device (smartphone), Dual-Tone Multi-Frequency (DTMF) decoder, an Arduino 16 MCU, sensors, relay modules, and the connected loads for experimental purposes. Their results obtained from the Proteus software environment show that the proposed design ensures high security against data and power theft since all home appliances are protected via an implemented password system.

To further increase the energy supplies for smart home environments, static solar panels were replaced by mobile PV systems that optimize their position depending on the Sun's movement during daylight cycles. A.D. Asham et al. [11] connected a dual-axis solar tracker to an Egyptian smart green home design where energy consumption is a persisting challenge. To address this issue, the authors proposed a two-folded methodology that targets power consumption monitoring and a dedicated solar power supply system that reduces the power consumption from the National Power Grid. Their proposed

system comprises a wireless network of controllers distributed in different areas of the home to monitor the energy consumption via a TFT Touchscreen actively. A similar smart home solution is found in [12], where a variety of deployed IoT devices (light switches, power plug, temperature sensor, gas sensor, water flow sensor, water level sensor, and motion sensors) are powered directly from sun-tracking solar panels. The feasibility and effectiveness of the author's proposed system demonstrate that future greenhouses will soon benefit entirely from solar energy, therefore becoming independent from the traditional power grid.

The previously described research efforts show that energy management remains a crucial element in intelligently distributing clean energy to power modern IoT-connected devices deployed in solar-powered smart home automation systems. A novel smart home energy management system is presented in [13], which relies on two algorithms, the Cost Saving Task Scheduling algorithm and the Renewable Source Power Allocation algorithm. By combining the two above-listed strategies, the authors achieve, with their proposed approach, an energy cost saving between 35% and 65% compared to test scenarios where automatic control is absent. A more optimized energy management strategy is presented in [14] where the authors propose a modern Home Energy Management System (HEMS) to economically manage the operation of a Home Energy Storage System (HESS), as well as minimize daily household energy costs, optimize PV self-consumption, and increase consumer benefits. Their proposed HEMS employs an optimization-based rolling horizon technique to determine the optimum HESS settings based on real-time measurements. The optimization process is run every two minutes to update the HESS settings. The experimental results of their design show a yearly household payment reduction of 32% and a yearly PV self-consumption of up to 87%. Finally, in [15], the authors propose a Smart Power Management (SPM) that aims to distribute power across consumers connected to a microgrid of interconnected Solar Home Systems (SHS) to improve the reliability and affordability of the supplied energy. Their experimental results show significant improvements in the reliability of power supplies within the microgrid infrastructure.

This paper distinguishes itself from the previous works by proposing a modified global energy production computation formula that replaces the traditional *PR* factor with a novel *SRF* parameter, which describes the reliability and availability of our solar tracking device. Hence, by varying the *SRF* parameter, we analyze the energy production equation in different scenarios, demonstrating that reliability-oriented metrics significantly improve the accuracy of predicting the energy production outcome and optimize energy management strategies of solar-powered smart home automation systems.

2. Proposed Energy Management Solution for the Smart Home Automation System

In this section, an efficient energy management diagram is proposed to improve the power distribution and achieve self-sufficiency for our solar-powered smart home automation system. The energy management design is constructed around two major modules: (a) solar tracking module with energy storage solution; (b) home automation model with energy storage solution and smart switching relay modules.

2.1. Solar Tracking Module with Energy Storage Solution

According to the literature review, one of the most important facilities of solar-powered smart home automation systems is the ability to power all deployed IoT-connected devices with clean energy to reduce the energy consumption of sensors, actuators, DC motors, etc. As shown in the top layer of Figure 1, we distinguish the Dual-Axis Solar Tracker block, which is composed of the PV panel, and the electrical equipment that optimizes the payload's position every hour during daylight cycles. The PV panel's role is to generate electrical energy for charging the power banks and other connected devices. The Solar Tracker block is linked to the INA219A module used to monitor the amount of energy produced by the solar panel by reading parameter values such as current, voltage, and power every 60 min.

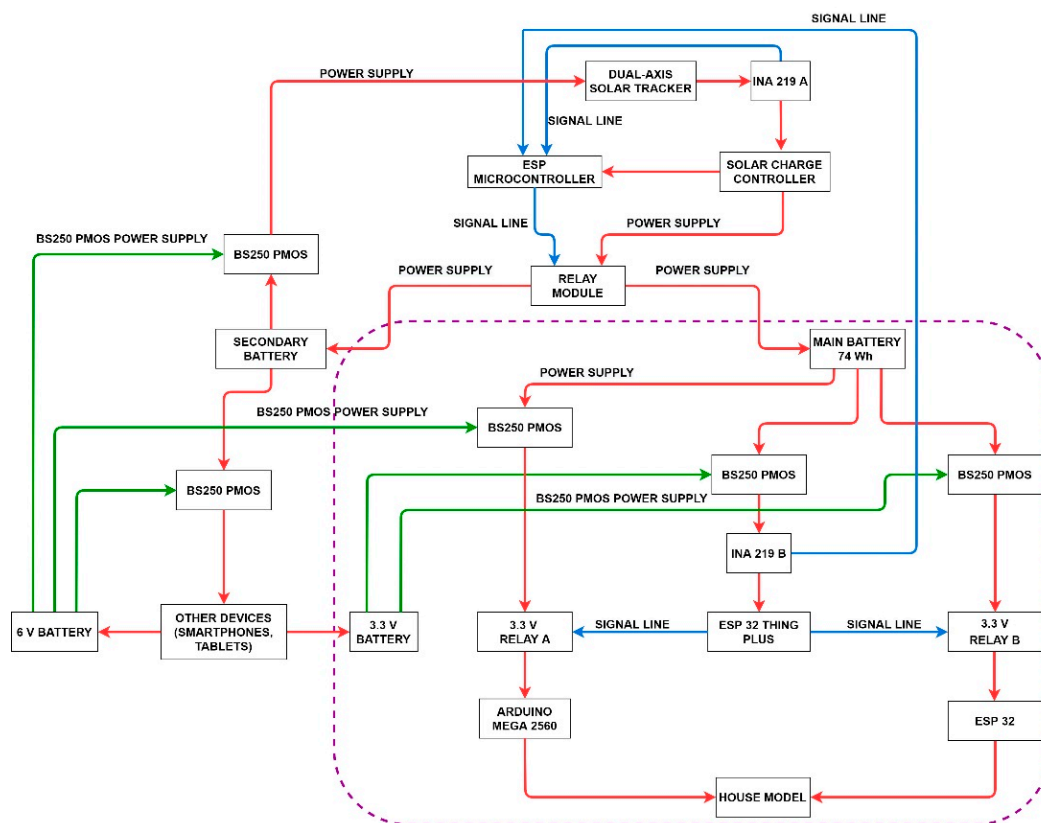


Figure 1. Proposed Energy Management Block Diagram for the Solar-Powered Smart Home Automation System.

The next element in the diagram is the Solar Charge Controller, which is utilized to regulate the energy flow from the PV array and to transfer it directly to the power banks as a DC-coupled system. The Solar Charge Controller provides energy for many components of the diagram, one of them being the ESP MCU (ESP 8266 or ESP 32) that sends data to Google Sheets, a cloud-based system that stores information obtained from the monitoring of energy generation of the PV panel, energy consumption of the smart home appliances, and the charging level of the power banks. The Solar Charge Controller is connected to a Relay module block, which transfers the solar panel's energy to the ESP MCU, the central power bank, and the secondary power bank.

The secondary battery's role is two-folded: first, it provides voltage supplies to the electrical equipment of the solar tracker; secondly, the surplus of stored energy can be used to power other devices such as smartphones and tablets, to name only a few. For clarity, the connections between the depicted elements in Figure 1 were labeled in the following manner: power supply lines were highlighted with red color, signal lines were marked with blue color, and transistor power supply lines were highlighted with green color.

2.2. Home Automation Model with Energy Storage Solution and Smart Switching Relay Modules

The second module of the energy management solution can be observed in the bottom part of Figure 1 (inside the purple dotted box) and continues with the main power bank description. The primary battery offers 3 USB ports and provides energy to 3 main development boards: Arduino Mega 2560 MCU, ESP 32 Thing Plus, ESP 32 MCU, and all sensor modules mounted inside the smart home automation system. The INA219B IoT device is used to monitor the main battery's discharging level and gives proper feedback to the ESP MCU from the Solar Tracking module layer. The Arduino Mega 2560 is the main MCU and is used to control the sensors, micro servo motors, and the other devices installed inside the House Model. On the other hand, the ESP32 MCU is connected to the sensor modules and enables remote control via a smartphone with Wi-Fi capabilities.

The ESP 32 Thing Plus is deployed to control a pair of relay modules remotely: Relay A, which is used to turn on and off the Arduino Mega 2560 MCU, and Relay B is utilized to turn on and off the ESP 32 MCU. The smart switching relay method will ensure proper maintainability when one sensor module becomes faulty during operation and requires replacement. Additionally, BS250 PMOS transistors are distributed between several block elements of the diagram to maintain a constant voltage flow. Finally, the House model contains a series of sensor modules: MQ5 gas sensor (gas leakage detection), water sensor (flood detection), DHT22 sensor (temperature and humidity monitoring), flame sensor (fire detection), light sensor (level of light inside the home), piezoelectric sensor (for detecting movement inside the house), and motors (MG 90 S servo motor which is used to automatically open and close the door if a valid tag with access rights is presented to the RFID module).

3. Proposed Reliability-Oriented Metrics for Computing the Energy Production of the Solar-Powered Smart Home Automation System

In the following, we detail the proposed reliability-oriented metrics necessary for computing the energy production of the solar-powered home automation system seen earlier in Figure 1, as well as alternative formulas for establishing the energy generation of state-of-the-art PV systems.

3.1. Reliability-Oriented Metrics Applied in the Global Energy Production Formula

Reliability and availability metrics are essential quality indicators for evaluating the performance of modern solar tracking systems. More precisely, our novel reliability metrics proposed in [16] employ an *STF*, which aims to use data from different test scenarios (software, hardware, and ICT) for computing the fault coverage, as well as an *SRF* that generates a probabilistic reliability parameter based on the precomputed *STF*.

As formulated in [16], the general form of the *STF* parameter is presented in Equation (1):

$$STF = \frac{N_E \times T_V}{T_P \times 2^N} \quad (1)$$

where T_V denotes the number of executed test vectors, N_E denotes the number of errors per test case, T_P denotes the total number of test patterns, and N denotes the number of similar devices used for error detection. At the same time, its variations depend mainly on the nature of test scenarios. For instance, in the case of hardware error detection, we can quickly adapt the general formula as depicted in relation (2) [16]:

$$STF_H = \frac{N_E \times T_V}{T_P \times 2^D} \quad (2)$$

where D stands for the total number of flip-flops used in Built-In Self-Test (BIST) routines. Similarly to hardware testing, when considering software test case scenarios, we can modify the general formula as presented in Equation (3) [16]:

$$STF_S = \frac{N_E \times T_V}{T_P \times 2^B} \quad (3)$$

where B represents the number of software functions/breakpoints implemented in White-Box Software Testing (WBST) routines. Moreover, when employing ICT test scenarios, the general *STF* formula is written according to Equation (4) [16]:

$$STF_I = \frac{N_E \times T_R}{N_R \times 2^P} \quad (4)$$

where N_R represents the total number of test rounds, and P designates the number of equipped probes during the ICT method. To include all test scenarios into one compact

global equation set, we apply a unified metrics system, as described in [8], according to equation set (5):

$$\begin{cases} STF_G = \frac{STF_H + STF_S + STF_I}{\frac{N_E \times T_V}{T_P \times 2^D} + \frac{N_E \times T_V}{T_P \times 2^B} + \frac{N_E \times T_R}{N_R \times 2^P}} \\ STF_G = \frac{STF_H + STF_S + STF_I}{n} \end{cases} \quad (5)$$

where STF_G represents the global solar test factor for mixed test scenarios, measured as the average value of all previously computed STF parameters, and n denotes the total number of STF parameters. Equally, as stated in [16], the general form of the SRF parameter is presented in Equation (6):

$$SRF = \exp\left[\frac{N_E \times T_V}{T_P \times 2^N}\right] \quad (6)$$

where exp stands for Euler's constant with a default value of $e = 2.71828$. Furthermore, the SRF parameter can be computed for each of the predefined STF variables from Equations (2)–(4), obtaining the global equation system (7) [8]:

$$\begin{cases} SRF_G = \frac{SRF_H + SRF_S + SRF_I}{\exp\left[\frac{N_E \times T_V}{T_P \times 2^D}\right] + \exp\left[\frac{N_E \times T_V}{T_P \times 2^B}\right] + \exp\left[\frac{N_E \times T_V}{T_P \times 2^P}\right]} \\ SRF_G = \frac{SRF_H + SRF_S + SRF_I}{n} \end{cases} \quad (7)$$

where SRF_G represents the global solar reliability factor for mixed test scenarios, measured as the average value of all previously computed SRF parameters, and n denotes the total number of SRF parameters.

Although the previously described unified metric systems are essential for assessing the performance of robust and durable solar tracking systems [8,16], in the context of this paper its applicability is extended to the energy production domain. More precisely, we aim to improve the global energy production formula by replacing the traditional PR factor with the above-computed global SRF parameter and increasing the prediction of the solar tracker's energy generation.

Regarding the solar energy generation domain, the global formula for estimating the generated electricity at the output of a PV system can be expressed as in Equation (8):

$$E_p = A \times r \times H \times PR \quad (8)$$

where E_p represents the energy production expressed in Wh, A represents the total solar panel area in cm^2 , r represents the solar panel yield in percent, H represents the annual average solar radiation on static solar panels (shadings not included), and PR represents the output ratio coefficient for losses (range between 0.5 and 0.9), with a default value of 0.75). Supplementary parameter r is given by the ratio of electrical power (expressed in Wp) of one solar panel divided by the panel's functional area. Mathematically, the yield r can be written as in Equation (9):

$$r = \frac{P}{S} \quad (9)$$

where P is the outputted power of the solar panel divided by the functional area S . Furthermore, the parameter P can be extended as in relation (10):

$$P = U \times I \quad (10)$$

where U represents the voltage expressed in V (volts), and I is the current collected from all PV cells and is expressed in A (amperes).

However, in real-time test scenarios, certain weather conditions impact the solar panel's performance, resulting in significant voltage loss, one example here being the temperature. Similar to other electronic components, in cold temperatures solar panels operate more effectively, allowing the panel to generate more voltage and, therefore, more electricity. As the temperature increases, the panel produces less voltage and becomes less effective, resulting in less produced electricity, as shown in Figure 2.

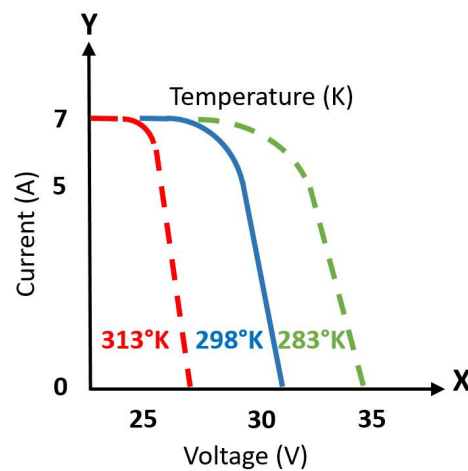


Figure 2. Ideal, Standard, and Critical Temperature Variation.

Figure 2 presents the voltage (X-Axis)-current (Y-Axis) dependencies based on the ideal (green-dotted line), standard (blue line), and critical (red-dotted line) temperature variations. The collected values from Figure 2 are extracted from various tests conducted by manufacturers in the PV market, demonstrating that, in general, for each degree above 298 degrees Kelvin (K), known as a Standard Testing Condition (STC), the solar panel will become one percent less efficient.

However, the voltage produced from the above graphical representation in Figure 2 depends on the solar panel configuration (total voltage output), an aspect which will be detailed in Section 4 of this paper. The temperature’s impact on the voltage parameter from Equation (10) can be expressed mathematically as in relation (11):

$$U(T) = U - (T - 298)\% \times U \quad T \in [298 \text{ K}; 338 \text{ K}] \tag{11}$$

where U is the voltage expressed as a function of the temperature T . By combining relations (7)–(11), we obtain the equation system (12):

$$\begin{cases} E_P = A \times r \times H \times PR \\ r = \frac{P}{S} \\ P = U \times I \\ U(T) = U - (T - 298)\% \times U \quad T \in [298 \text{ K}; 338 \text{ K}] \\ PR = SRF_G \\ SRF_G = \frac{SRF_H + SRF_S + SRF_I}{n} \end{cases} \tag{12}$$

By compressing equation system (12), we obtain the final global energy production formula (13):

$$E_P = A \times \frac{[U - (T - 298)\% \times U] \times I}{S} \times H \times SRF_G \quad T \in [298 \text{ K}; 338 \text{ K}] \tag{13}$$

where the temperature T takes values between 298 K and 338 K. If the parameter T is lower than 25 °C, there will be no PV panel voltage losses. For a more concrete example, let us consider a real-life scenario where we gradually substitute each variable according to formula (12).

First, we calculate the global *STF* by considering three test scenarios for BIST, WBST, and ICT routines.

Regarding BIST test scenarios, we will start from the following considerations: (a) for a total number of $T_V = 7$ (test cases), we have successfully identified $N_E = 10$ bit-flip errors. Concerning property (a), since multiple errors (burst errors) may occur within a single test vector, the number of errors detected may be greater than the number of test cases [16]. Additionally, we have (b) a number $D = 4$ flip flops used in the structure of a random

Multiple Input Signature Register (MISR). The proposed formula is used to measure the total number of test cases T_P , as presented in Equation (14) [16]:

$$T_P = 2^D - 1 \rightarrow T_P = 2^4 - 1 = 15 \quad (14)$$

By having this hypothetical data, we will be able to substitute the variables from Equation (2) in relation (15) [16]:

$$STF_H = \frac{10 \times 7}{15 \times 16} = \frac{70}{240} = 0.29 \approx 0.30 \quad (15)$$

Regarding WBST routines, we will start from the following considerations: (a) for a total number $T_V = 7$ (test cases), we have successfully identified $N_E = 10$ calculation errors. Additionally, we have: (b) a number of $T_P = 10$ test patterns and a number $B = 10$ breakpoints in our software code, meaning that all calculation errors were successfully detected using the deployed software functions. Let us proceed with computing the STF parameter, as presented in Equation (16) [16]:

$$STF_S = \frac{10 \times 7}{10 \times 10} = \frac{70}{100} = 0.70 \quad (16)$$

Regarding ICT routines, let us consider a real-life scenario where we want to identify all possible test points' voltage deviations. For this purpose, we implement a total of $T_R = 100$ test routines, a total of $N_R = 10$ rounds for each test stage, and $P = 2$ probes to classify $N_E = 12$ voltage deviations. Based on the previous configuration, the STF parameter will be computed using relation (17) [16]:

$$STF_I = \frac{N_E \times T_R}{N_R \times 2^P} = \frac{12 \times 10}{100 \times 2^2} = \frac{120}{400} = 0.30 \quad (17)$$

At this point, we can apply equation set (5) to compute the global STF parameter, as presented in expression (18):

$$\begin{cases} STF_G = \frac{STF_H + STF_S + STF_I}{3} \\ STF_G = \frac{0.30 + 0.70 + 0.30}{3} = \frac{1.3}{3} = 0.43 \end{cases} \quad (18)$$

Secondly, according to equation system (8), we can calculate the global SRF by following a series of steps. Since the SRF expression is the STF equation's exponential, we can rewrite the entire relationship as in Equation (19):

$$\begin{cases} SRF_{H,I} = e^{-STF_{H,I}} = e^{-0.3} = \frac{1}{e^{0.3}} = \frac{1}{2.71^{0.3}} = \frac{1}{1.3486} = 0.74 \\ SRF_S = e^{-STF_S} = e^{-0.7} = \frac{1}{e^{0.7}} = \frac{1}{2.71^{0.7}} = \frac{1}{2} = 0.50 \end{cases} \quad (19)$$

At this point, we can compute the global SRF of the automated solar tracking equipment as presented in Equation (20):

$$\begin{cases} SRF_G = \frac{e^{-STF_H} + e^{-STF_S} + e^{-STF_I}}{3} \\ SRF_G = \frac{0.74 \times 2 + 0.50}{3} = \frac{1.98}{3} = 0.66 \end{cases} \quad (20)$$

Conclusively, the global SRF is rated at 66% when the solar tracking system is affected by hardware, software, and in-circuit errors.

3.2. Global Energy Production Formula Applied to Real-Life Scenarios

The metrics mentioned above can be applied to various real-life scenarios regarding the calculus of reliability, availability, and global energy production. More specifically, to establish accurate predictions about the global energy production of the entire solar-powered smart home automation system, we are interested in formulating problems

concerning the error rates and power generation of the solar tracker. For instance, let us consider the precomputed global SRF parameter, which is used to assess the reliability of the solar tracking equipment, and we want to determine the power output, respectively, the global energy production for one complete day cycle. We can solve this problem by just relying on equation set (14) and by following the subsequent considerations: (a) for simplicity, the total area of the solar panel A is equal to the usable surface of the PV panel S ; (b) during one daylight cycle measurements were performed according to the STC from Section 3.1, obtaining a solar panel output voltage of 12 V and a current flow of 0.6 A, with a constant temperature $T = 298$ K, and under a solar irradiance level of $H = 1$ kW per square meter. By substituting all known variables with their determined values, we obtain the following results, as presented in equation set (21):

$$\begin{aligned} E_P &= A \times \frac{[U-(T-298)\% \times U] \times I}{S} \times H \times SRF_G \\ E_P &= A \times \frac{[12-(298-298)\% \times 12] \times 0.6}{A} \times 1 \times 0.66 \\ E_P &= 12 \times 0.6 \times 1 \times 0.66 = 4.752 \text{ Wh} \\ T &\in [298 \text{ K}; 338 \text{ K}] \end{aligned} \quad (21)$$

Let us further consider that the solar tracking device is not harmed by system errors and works in optimal conditions. Under these circumstances, the global SRF parameter will be rated at 100%, resulting in the equation system (22):

$$\begin{aligned} E_P &= A \times \frac{[U-(T-298)\% \times U] \times I}{S} \times H \times SRF_G \\ E_P &= A \times \frac{[12-(298-298)\% \times 12] \times 0.6}{A} \times 1 \times 1 \\ E_P &= 12 \times 0.6 \times 1 \times 1 = 7.2 \text{ Wh} \\ T &\in [298 \text{ K}; 338 \text{ K}] \end{aligned} \quad (22)$$

Hence, when the global SRF is 1, it does not impact the global energy production of the entire solar-powered smart home automation system.

3.3. Alternative Formulas for Calculating the Global Energy Production of PV systems

Besides the proposed reliability metrics, which improve the accuracy of computing the global energy production, there are several state-of-the-art methodologies [17,18] in the solar energy domain which allow increased prediction in determining the long-term energy production of modern PV systems.

Similar to our previously described model, several parameters reappear in literature formulas, such as the PR factor [17], which is considered a critical parameter for evaluating PV output since it summarizes the deviation from the STC, the various losses due to device equipment (such as inverters, cables, etc.), and the effect of multiple variables (radiation incidence angle, temperature, soiling, etc.). The PR factor is computed using the formula (23) [17]:

$$PR = k_{\theta} \times k_Q \times k_{B1} \times k_{\gamma} \times k_W \times k_S \times \eta_{inv} \quad (23)$$

where k_{θ} is the optical reflection reduction factor; k_Q is the quantum efficiency reduction factor; k_{B1} is the low irradiance reduction factor; k_{γ} is the module temperature reduction factor; k_W is the wiring losses reduction factor; k_S is the soiling factor; η_{inv} is the inverter conversion efficiency. The losses due to the temperature of cells can be calculated, at every time step, with Equation (24) [17]:

$$k_{\gamma} = \frac{100 - \gamma(T_C - T_{ref})}{100} \quad (24)$$

where γ is the power temperature factor [%/°C]; T_C is the temperature of the PV cells [°C]; T_{ref} is the cell's reference temperature [°C]. Regarding the previous formula, the reference temperature for the cell is 25 °C, and the temperature factor γ is referred to the energy provided by the PV module; the value of which is a variable of the particular type of module and the semiconductor that composes the cells, usually ranging between 0.2 and

0.5. The temperature T_C of the PV cell is measured as a function of ambient temperature, irradiance, and NOCT parameter and is computed with Equation (25) [17]:

$$T_C = T_a + \frac{NOCT - 20}{0.8} \times G_T \quad (25)$$

where T_a is the ambient temperature (in degrees Celsius); $NOCT$ is the nominal operating cell temperature [$^{\circ}\text{C}$]; G_T is the global irradiance on the surface of the module [kW/m^2]. Most of the above-described factors are affecting the performance of PV systems. For the correlation of these variables, multiple mathematical equations are used, all of which are linked to the fundamental formula (26) [17]:

$$E_{PV} = PR \times P_n \times \frac{H_T}{G_{STC}} \quad (26)$$

where E_{PV} is the amount of electricity produced by the PV system during the analysis time [kWh]; PR is the solar plant's output ratio; P_n is the plant's nominal power, calculated in STC [kW]; G_{STC} is the solar irradiance in STC [kW/m^2]; H_T is the total solar irradiation on the modules plan [kWh/m^2]. Formula (26) can be used to estimate PV output over long periods (day, month, year), but it can also be utilized for instant calculations. The inverter efficiency function can then be expressed using Equation (27) [17]:

$$\eta_{inv} = (aPLR^2 + bPLR + c) \times \log(PLR \times 10^3 - d) \quad (27)$$

where η_{inv} is the inverter efficiency; PLR is the component load ratio; and a, b, c, d are precomputed nonlinear regression coefficients. Furthermore, the PLR of inverter operation is calculated using the Equation (28) [17]:

$$PLR = \frac{P_{inv}}{P_{inv,nom}} \quad (28)$$

where P_{inv} is the inverter's power output [kW]; $P_{inv, nom}$ is the inverter's nominal power output [kW]. The parameters chosen are the most important for PV output, and therefore it is possible to define an energy estimation formula, as presented in relation (29) [17]:

$$E_{PV,year,est} = aH_{T,hor} + bT_m + c\Upsilon + d \quad (29)$$

where $E_{PV,year,est}$ is an estimate of the electricity produced by a 1 kWp PV system in one year [kWh]; $H_{T,hor}$ is the average solar irradiation of the modules over a year [kWh/m^2]; T_m denotes the annual average air temperature [$^{\circ}\text{C}$], and Υ is the power temperature coefficient [$\%/^{\circ}\text{C}$]. A reliability ratio formula is finally used to compare the measured energy production with the estimated energy production, as illustrated in Equation (30):

$$Ratio = \frac{E_{PV,year}}{E_{PV,year,est}} \quad (30)$$

where $E_{PV,year}$ is the yearly measured energy PV production [kWh]; $E_{PV,year,est}$ is the yearly estimated PV production. The reliability ratio calculated for accurate data remains in the level of accuracy generally attributed to PV simulation tools [17].

A simplified energy production computation model is presented in [18] where the solar-generated power (Watt Peak) is calculated with the formula (31):

$$P_{Watt\ Peak} = Area\ array \times PSI \times \eta_{PV} \quad (31)$$

where $P_{Watt\ Peak}$ is the maximum power generation of the PV panel; $Area\ Array$ is the usable surface equipped with PV cells; PSI is the peak sun insolation (solar radiation), and η_{PV} represents the solar panel efficiency. For a more concrete example, let us consider that the $Array\ area$ is $50\ \text{m}^2$, PSI is rated at $1000\ \text{W}/\text{m}^2$, and the solar panel efficiency is 17%. The

above-listed assumptions were made for STC where solar cell efficiency η_{PV} is defined between 15% and 17%, at a temperature of 25 °C, resulting in the equation set (32) [18]:

$$P_{Watt\ Peak} = 50\text{ m}^2 \times 1000\text{ W/m}^2 \times 0.17 = 8.750\text{ Wp} \quad (32)$$

Additionally, if multiple solar panels are connected to the same grid, we can compute the total number of solar panels, with a maximum output power of 130 Wp per panel, by using the formula (33):

$$N_{SP} = \frac{P_{watt\ peak}}{P_m} = \frac{8.750\text{ W}}{130\text{ W}} = 67.30 \approx 68\text{ solar panels} \quad (33)$$

where P_m is the maximum outputted power by a solar panel.

4. Experimental Setup and Results

This section of the paper is divided into two subchapters comprising the hardware implementation and Cloud layer of the solar-powered smart home automation system, as well as a comparison between our proposed global energy production formula based on reliability-oriented metrics and alternative energy production equations from related works.

4.1. Hardware Implementation and Cloud Layer of the Solar-Powered Smart Home Automation System

As previously described in Section 2, the hardware setup of the solar-powered smart home automation system is divaricated into two major parts: the solar tracking module [19] and the smart home automation module [20]. The first element shows the dual-axis solar tracker (a) that powers the smart home automation system; its maximum power output, as well as other parameters, are outlined in the subsequent subchapter of this section. The next component is the solar charge controller (b), a powerful all-in-one control device that provides three input-output ports: one dedicated to solar modules, one dedicated to charging the PV panel battery with collected electricity from the solar panel's PV cells, and one output module for connecting the current charge. The Ultra Cell battery (c) is a 12 V, 9 Ah acid-plumb battery, which is often used in UPS systems to provide energy for desktop computers in the event of a local power failure. Distinct from the block diagram in Figure 1, we connected a DC-to-DC inverter (d) between the battery and the dual-axis solar tracker to power the electrical equipment directly from the accumulator. Since the *SRF* parameter can only be obtained from the fault coverage of intrusive system errors, we connected the solar tracking equipment to a dedicated Hybrid Testing Platform (e) composed of a Flying Probe In-Circuit Tester (FPICT) and an ST-Link V2 JTAG module adapter [21], as shown in Figure 3.

Additionally, for monitoring the FPICT process and the JTAG method, we made use of a Raspberry Pi 3B+ (f) as our primary computing platform as well as a 7-inch display (g) for visualizing the results of our test cases.

According to the block diagram depicted in Figure 1, the main development board connecting the hardware layer of the solar-powered smart home automation system with the Cloud layer is the ESP32 Thing Plus Wi-Fi module (i). We opted for the low-cost and low-power ESP32 MCU due to the integrated Wi-Fi and Bluetooth capabilities which operate at long-range distances, one additional benefit being the power-management modules that reduce the energy consumption considerably. The ESP32 makes use of its Wi-Fi capabilities to transfer data received from the solar tracker to the specifically created Google Sheet and is also used to divert the flow of energy obtained from the solar tracking device to the required equipment based on the outcome of the obtained and stored results in Google Sheet. The first element in the Cloud layer is Google Drive (j), a cloud storage environment used to store information and data transferred from the weather website to Google Sheets via an add-on called Coupler.io. The data from the solar tracking

device is also transferred to Google Drive with a secondary ESP 32 MCU, as depicted in Figure 1. All the stored data from the weather and the solar tracker, combined with personalized mathematical formulas, is used to monitor, predict, and control the flow of electrical energy for the solar-powered home automation system. The second element is the Coupler.io add-on (k), a software interface that can be easily integrated into the Cloud system via Google Sheets and has the role to pull the required data from the weather website on a fixed schedule (in our case, every day from 4:00 a.m. to 11:00 p.m.). Since the employed Coupler.io is a free variant, we can only pull 50,000 rows of data per month, which is more than sufficient because we need less than 744 rows per month for our hourly monitoring. The third element in the Cloud layer depicts the website from which weather data is collected in real time, using a dedicated Application Programming Interface (API) (l), which returns real-time weather conditions data for a specific location. The utilized API is provided by the weather website Accuweather and is free of charge for up to 50 calls per day, which is more than sufficient since we require less than 24 calls per day because we collect data only at specific times during 24 h. Finally, the hardware layer's last element represents the solar-powered home automation system (m) which will use the energy generated by the solar tracker to power all of its automated equipment and sensor components.

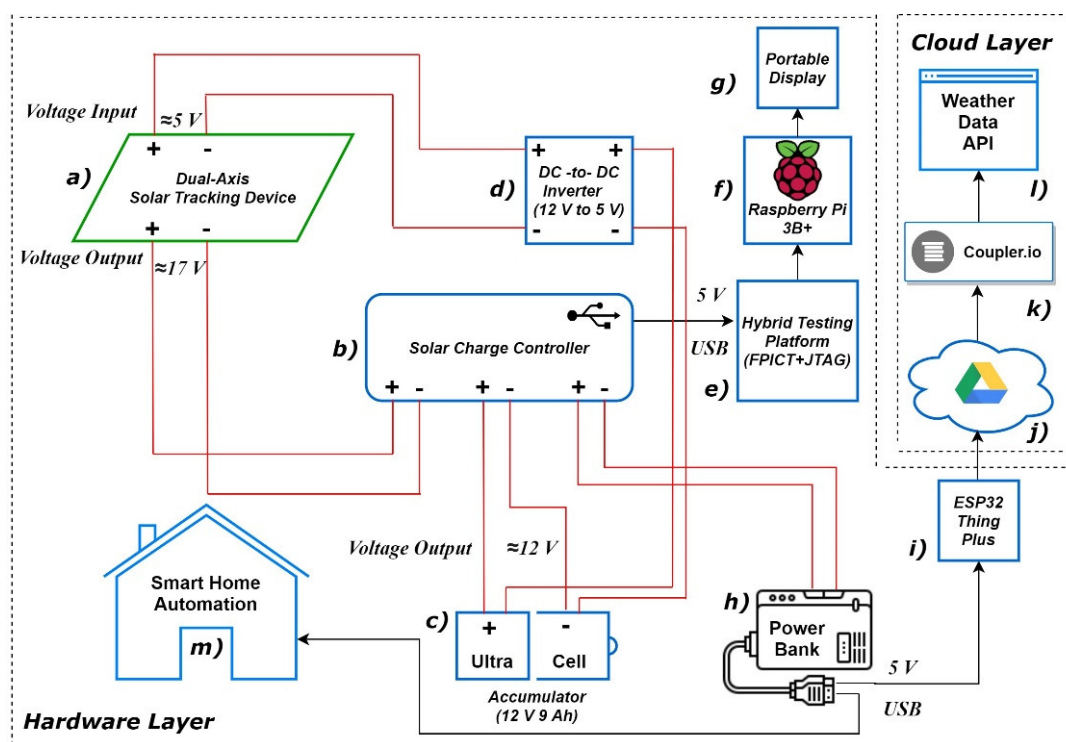


Figure 3. Conceptual Diagram of the Proposed Solar-Powered Smart Home Automation System with integrated Cloud Platform and Testing Facilities.

4.2. Energy Production Graphical Representations and Results

Our research investigates the global energy production efficiency variation concerning the computed *SRF* parameter that indicates the availability of the dual-axis solar tracking system. Traditional parameters such as voltage, current, power, solar radiation, and temperature are, however, not sufficient for plotting the graphical representations of the global energy production. Two additional coefficients are necessary for determining the global reliability factor of the solar tracking equipment, namely the *STF* and *SRF* parameters. In a previous work [8], we computed the global *STF* and *SRF* by using experimental error data (hardware, software, and in-circuit errors) gathered over two weeks, as presented in Table 1.

Table 1. Experimental results regarding our Hybrid Testing Suite (FPICT + JTAG) [21].

		Test Schedule		Fault Coverage (%)		
No. of Days		No. of Test Cases Per Day		Syntax Errors	Error Types	
		8:00 a.m.	4:00 p.m.		Structural Faults	Stuck-at-Faults
Mostly Sunny Week	1			70.20	78.20	60.10
	2			69.10	77.10	65.10
	3			65.14	65.20	69.15
	4	1	1	67.20	66.20	56.10
	5			66.66	60.20	55.45
	6			71.13	79.90	59.10
	7			65.20	75.13	52.01
Partly Cloudy Week	1			69.65	77.65	62.55
	2			67.67	71.70	64.62
	3			68.70	72.70	58.10
	4	1	1	68.43	72.20	57.27
	5			70.66	69.20	64.12
	6			67.70	71.65	54.10
	7			71.16	66.20	57.30
Total		28		67.80	Average Fault Coverage 71.70	59.57

First, regarding the mostly sunny week, according to relation (5) we calculated the equation set for the global STF parameters as expressed in the equation system (34) [8]:

$$\left\{ \begin{array}{l} STF_G = \frac{STF_H + STF_S + STF_I}{3} \\ STF_G = \frac{\frac{E_H}{2^D \times (2^D - 1)} + \frac{E_S}{T_P \times 2^B} + \frac{E_I}{N_R \times 2^P}}{3} \\ STF_{G1} = \frac{\frac{E_{H1}}{2^D \times (2^D - 1)} + \frac{E_{S1}}{T_P \times 2^B} + \frac{E_{I1}}{N_R \times 2^P}}{3} \\ STF_{G2} = \frac{\frac{E_{H2}}{2^D \times (2^D - 1)} + \frac{E_{S2}}{T_P \times 2^B} + \frac{E_{I2}}{N_R \times 2^P}}{3} \\ STF_{G3} = \frac{\frac{E_{H3}}{2^D \times (2^D - 1)} + \frac{E_{S3}}{T_P \times 2^B} + \frac{E_{I3}}{N_R \times 2^P}}{3} \\ STF_{G4} = \frac{\frac{E_{H4}}{2^D \times (2^D - 1)} + \frac{E_{S4}}{T_P \times 2^B} + \frac{E_{I4}}{N_R \times 2^P}}{3} \\ STF_{G5} = \frac{\frac{E_{H5}}{2^D \times (2^D - 1)} + \frac{E_{S5}}{T_P \times 2^B} + \frac{E_{I5}}{N_R \times 2^P}}{3} \\ STF_{G6} = \frac{\frac{E_{H6}}{2^D \times (2^D - 1)} + \frac{E_{S6}}{T_P \times 2^B} + \frac{E_{I6}}{N_R \times 2^P}}{3} \\ STF_{G7} = \frac{\frac{E_{H7}}{2^D \times (2^D - 1)} + \frac{E_{S7}}{T_P \times 2^B} + \frac{E_{I7}}{N_R \times 2^P}}{3} \end{array} \right. \quad (34)$$

where E_H stands for the hardware error data from column 7 of Table 1, E_S designates the software error data from column 5 of Table 1, and E_I represents the in-circuit error data from column 6 of Table 1. The above metrics system were calculated for a number of $D = 16$ flip-flops (for stuck-at-faults), $T_P = 840$ (for syntax errors), and $N_R = 1000$ (for structural faults). Accordingly, we obtained the following results, presented in equation system (35) [8]:

$$\left\{ \begin{array}{l} STF_{G1} = \frac{0.6010 + 0.0219 + 0.391}{3} = \frac{1.0139}{3} = 0.33796 \\ STF_{G2} = \frac{0.6510 + 0.0215 + 0.3855}{3} = \frac{1.058}{3} = 0.3526 \\ STF_{G3} = \frac{0.6915 + 0.0203 + 0.326}{3} = \frac{1.0378}{3} = 0.34593 \\ STF_{G4} = \frac{0.5610 + 0.021 + 0.331}{3} = \frac{0.913}{3} = 0.3043 \\ STF_{G5} = \frac{0.5545 + 0.020 + 0.301}{3} = \frac{0.8755}{3} = 0.2918 \\ STF_{G6} = \frac{0.5910 + 0.022 + 0.3756}{3} = \frac{0.9886}{3} = 0.2918 \\ STF_{G7} = \frac{0.5201 + 0.020 + 0.3755}{3} = \frac{0.9156}{3} = 0.3052 \end{array} \right. \quad (35)$$

Similarly, concerning the partly cloudy week, we computed the global *STF* parameters, as presented in equation set (36) [8]:

$$\left\{ \begin{array}{l} STF_G = \frac{STF_H + STF_S + STF_I}{3} \\ STF_G = \frac{\frac{E_H}{2^D \times (2^D - 1)} + \frac{E_S}{T_P \times 2^B} + \frac{E_I}{N_R \times 2^P}}{3} \\ STF_{G8} = \frac{\frac{E_{H8}}{2^D \times (2^D - 1)} + \frac{E_{S8}}{T_P \times 2^B} + \frac{E_{I8}}{N_R \times 2^P}}{3} \\ STF_{G9} = \frac{\frac{E_{H9}}{2^D \times (2^D - 1)} + \frac{E_{S9}}{T_P \times 2^B} + \frac{E_{I9}}{N_R \times 2^P}}{3} \\ STF_{G10} = \frac{\frac{E_{H10}}{2^D \times (2^D - 1)} + \frac{E_{S10}}{T_P \times 2^B} + \frac{E_{I10}}{N_R \times 2^P}}{3} \\ STF_{G11} = \frac{\frac{E_{H11}}{2^D \times (2^D - 1)} + \frac{E_{S11}}{T_P \times 2^B} + \frac{E_{I11}}{N_R \times 2^P}}{3} \\ STF_{G12} = \frac{\frac{E_{H12}}{2^D \times (2^D - 1)} + \frac{E_{S12}}{T_P \times 2^B} + \frac{E_{I12}}{N_R \times 2^P}}{3} \\ STF_{G13} = \frac{\frac{E_{H13}}{2^D \times (2^D - 1)} + \frac{E_{S13}}{T_P \times 2^B} + \frac{E_{I13}}{N_R \times 2^P}}{3} \\ STF_{G14} = \frac{\frac{E_{H14}}{2^D \times (2^D - 1)} + \frac{E_{S14}}{T_P \times 2^B} + \frac{E_{I14}}{N_R \times 2^P}}{3} \end{array} \right. \quad (36)$$

The *STF* parameters for the partially cloudy week were determined for a number $D = 16$ flip-flops, $T_P = 840$ software test vectors, $N_R = 1000$ in-circuit routines, according to the equation set (37) [8]:

$$\left\{ \begin{array}{l} STF_{G8} = \frac{0.6255 + 0.0217 + 0.3882}{3} = 0.3451 \\ STF_{G9} = \frac{0.6462 + 0.0211 + 0.3585}{3} = 0.3419 \\ STF_{G10} = \frac{0.5810 + 0.0214 + 0.3635}{3} = 0.3219 \\ STF_{G11} = \frac{0.5727 + 0.0213 + 0.361}{3} = 0.3183 \\ STF_{G12} = \frac{0.5727 + 0.0228 + 0.346}{3} = 0.3364 \\ STF_{G13} = \frac{0.5410 + 0.0211 + 0.358}{3} = 0.3068 \\ STF_{G14} = \frac{0.5730 + 0.0222 + 0.331}{3} = 0.3087 \end{array} \right. \quad (37)$$

Secondly, according to equation set (7) and the determined global *STF* values, we computed the global *SRF* parameters for the mostly sunny week, as presented in equation system (38) [8]:

$$\left\{ \begin{array}{l} SRF_G = \frac{SRF_H + SRF_S + SRF_I}{3} \\ SRF_G = \frac{\exp[\frac{E}{2^D \times (2^D - 1)}] + \exp[\frac{E}{T_P \times 2^B}] + \exp[\frac{E}{N_R \times 2^P}]}{3} \\ SRF_{G1} = \frac{e^{-STF_{H1}} + e^{-STF_{S1}} + e^{-STF_{I1}}}{3} \\ SRF_{G2} = \frac{e^{-STF_{H2}} + e^{-STF_{S2}} + e^{-STF_{I2}}}{3} \\ SRF_{G3} = \frac{e^{-STF_{H3}} + e^{-STF_{S3}} + e^{-STF_{I3}}}{3} \\ SRF_{G4} = \frac{e^{-STF_{H4}} + e^{-STF_{S4}} + e^{-STF_{I4}}}{3} \\ SRF_{G5} = \frac{e^{-STF_{H5}} + e^{-STF_{S5}} + e^{-STF_{I5}}}{3} \\ SRF_{G6} = \frac{e^{-STF_{H6}} + e^{-STF_{S6}} + e^{-STF_{I6}}}{3} \\ SRF_{G7} = \frac{e^{-STF_{H7}} + e^{-STF_{S7}} + e^{-STF_{I7}}}{3} \end{array} \right. \quad (38)$$

By replacing the computed *STF* parameters in the metrics system (39), we obtained the *SRF* parameters, as presented in equation set (39) [8]:

$$\left\{ \begin{array}{l} SRF_{G1} = \frac{0.5482+0.9783+0.6763}{3} = 0.7342 \\ SRF_{G2} = \frac{0.5215+0.9787+0.6801}{3} = 0.7267 \\ SRF_{G3} = \frac{0.5008+0.9799+0.7218}{3} = 0.7341 \\ SRF_{G4} = \frac{0.5706+0.9792+0.7182}{3} = 0.756 \\ SRF_{G5} = \frac{0.5743+0.9801+0.7400}{3} = 0.7648 \\ SRF_{G6} = \frac{0.5537+0.9782+0.6868}{3} = 0.7395 \\ SRF_{G7} = \frac{0.5944+0.9801+0.6869}{3} = 0.7538 \end{array} \right. \quad (39)$$

With regards to the partly cloudy week, the remaining *SRF* parameters were calculated with the equation system (40) [8]:

$$\left\{ \begin{array}{l} SRF_G = \frac{SRF_H+SRF_S+SRF_I}{3} \\ SRF_G = \frac{\exp[\frac{E}{2^D \times (2^D - 1)}] + \exp[\frac{E}{T_P \times 2^B}] + \exp[\frac{E}{N_R \times 2^P}]}{3} \\ SRF_{G8} = \frac{e^{-STF_{H8}} + e^{-STF_{S8}} + e^{-STF_{I8}}}{3} \\ SRF_{G9} = \frac{e^{-STF_{H9}} + e^{-STF_{S9}} + e^{-STF_{I9}}}{3} \\ SRF_{G10} = \frac{e^{-STF_{H10}} + e^{-STF_{S10}} + e^{-STF_{I10}}}{3} \\ SRF_{G11} = \frac{e^{-STF_{H11}} + e^{-STF_{S11}} + e^{-STF_{I11}}}{3} \\ SRF_{G12} = \frac{e^{-STF_{H12}} + e^{-STF_{S12}} + e^{-STF_{I12}}}{3} \\ SRF_{G13} = \frac{e^{-STF_{H13}} + e^{-STF_{S13}} + e^{-STF_{I13}}}{3} \\ SRF_{G14} = \frac{e^{-STF_{H14}} + e^{-STF_{S14}} + e^{-STF_{I14}}}{3} \end{array} \right. \quad (40)$$

After solving the metrics system (41), we obtained the *SRF* parameters, as presented in equation set (41) [8]:

$$\left\{ \begin{array}{l} SRF_{G8} = \frac{0.5349+0.9784+0.6782}{3} = 0.7305 \\ SRF_{G9} = \frac{0.5240+0.9790+0.6987}{3} = 0.7339 \\ SRF_{G10} = \frac{0.5593+0.9787+0.6952}{3} = 0.7444 \\ SRF_{G11} = \frac{0.5639+0.9781+0.7075}{3} = 0.7374 \\ SRF_{G12} = \frac{0.5266+0.9801+0.7400}{3} = 0.7648 \\ SRF_{G13} = \frac{0.5821+0.9790+0.6988}{3} = 0.7533 \\ SRF_{G14} = \frac{0.5638+0.9780+0.7182}{3} = 0.7533 \end{array} \right. \quad (41)$$

Thirdly, based on equation set (5) and by analyzing the average values from Table 1, we accurately computed the general *STF* and *SRF* parameters according to the metrics system (42) [8]:

$$\left\{ \begin{array}{l} STF_G = \frac{0.5957+0.0211+0.358}{3} = 0.3251 \\ SRF_G = \frac{0.5511+0.9790+0.6987}{3} = 0.7429 \end{array} \right. \quad (42)$$

According to the last equation set (43), it is observable that the global *SRF* of the entire solar tracking device is rated at 74.29%.

Following this, we computed the global energy production of the solar tracking device according to the equation systems (12) and (13) in two different test scenarios. The first test scenario assumed that the mobile PV system operates in optimal conditions, thus implying that the $SRF_G = 1$ meaning that the solar tracker achieves 100% availability. Additional parameters such as the temperature coefficient and solar irradiance level were substituted according to their *STC* values. The second test scenario assumed that the mobile PV system was affected by operations errors hindering it from reaching its maximum harvesting potential. We replaced the *PR* factor with the computed *SRF* parameters to establish the global energy production of the solar tracking system according to its availability status. To monitor the impact of the *SRF*, the temperature, as well as the irradiance level, was kept

at their *STC* default values. The global energy production for the mostly sunny week was computed according to equation system (43):

$$\begin{cases} E_P = A \times \frac{[U-(T-298)\% \times U] \times I}{S} \times H \times SRF_G \\ E_{P1} = A \times \frac{[U_1-(T-298)\% \times U_1] \times I_1}{S} \times H \times SRF_G \\ E_{P2} = A \times \frac{[U_2-(T-298)\% \times U_2] \times I_2}{S} \times H \times SRF_G \\ E_{P3} = A \times \frac{[U_3-(T-298)\% \times U_3] \times I_3}{S} \times H \times SRF_G \\ E_{P4} = A \times \frac{[U_4-(T-298)\% \times U_4] \times I_4}{S} \times H \times SRF_G \\ E_{P5} = A \times \frac{[U_5-(T-298)\% \times U_5] \times I_5}{S} \times H \times SRF_G \\ E_{P6} = A \times \frac{[U_6-(T-298)\% \times U_6] \times I_6}{S} \times H \times SRF_G \\ E_{P7} = A \times \frac{[U_7-(T-298)\% \times U_7] \times I_7}{S} \times H \times SRF_G \\ T \in [298 \text{ K}; 338 \text{ K}] \end{cases} \quad (43)$$

Regarding the first test scenario, we considered the following values for the variables from equation system (14): the total area of the PV panel is equal to the usable PV cell surface ($A = S = 1548 \text{ cm}^2$); the temperature $T = 298 \text{ K}$; the solar radiation level is $H = 1 \text{ kW/m}^2$; the global reliability factor is $SRF_G = 1$. The measured voltage and current values were extracted from columns 4 and 5 of Table 2.

Table 2. Experimental results regarding Solar Panel Energy Generation and Storage, as well as System Energy Consumption during the Mostly Sunny Week [21].

Time	Solar Panel Output Voltage (V)	Solar Panel Output Current (A)	Accumulator Input Voltage (V)	Accumulator Charging Current (A)	Accumulator Discharging Current (A)	Solar Panel Power Gain (Wh)	System Energy Consumption (Wh)	UV Index
Day 1	17.33	1.2	12.5	0.88	0.45	10.97	8.21	7
Day 2	17.38	1.04	12.37	0.85	0.44	10.54	6.47	7
Day 3	17.31	0.94	12.38	0.85	0.46	10.55	6.72	7
Day 4	17.41	1.04	12.45	0.86	0.5	10.77	7.29	5
Day 5	16.79	0.84	12.44	0.8	0.56	9.99	8	5
Day 6	17.46	1.04	12.51	0.9	0.43	11.27	6.42	6
Day 7	17.45	1.05	12.55	0.89	0.46	11.23	6.8	6
Average	17.3042	1.0214	12.4571	0.8614	0.4714	10.76	7.13	6.1428

Hence, by replacing all variables with their default values, we obtained the global energy production for the mostly sunny week according to equation system (44):

$$\begin{cases} E_P = A \times \frac{[U-(T-298)\% \times U] \times I}{S} \times H \times SRF_G \\ E_{P1} = 1548 \times \frac{[12.5-(298-298)\% \times 12.5] \times 0.88}{1548} \times 1 \times 1 = 11 \\ E_{P2} = 1548 \times \frac{[12.37-(298-298)\% \times 12.37] \times 0.85}{1548} \times 1 \times 1 = 10.51 \\ E_{P3} = 1548 \times \frac{[12.38-(298-298)\% \times 12.38] \times 0.85}{1548} \times 1 \times 1 = 10.52 \\ E_{P4} = 1548 \times \frac{[12.45-(298-298)\% \times 12.45] \times 0.86}{1548} \times 1 \times 1 = 10.70 \\ E_{P5} = 1548 \times \frac{[12.44-(298-298)\% \times 12.44] \times 0.8}{1548} \times 1 \times 1 = 9.95 \\ E_{P6} = 1548 \times \frac{[12.51-(298-298)\% \times 12.5] \times 0.9}{1548} \times 1 \times 1 = 11.25 \\ E_{P7} = 1548 \times \frac{[12.55-(298-298)\% \times 12.55] \times 0.89}{1548} \times 1 \times 1 = 11.16 \\ T \in [298 \text{ K}; 338 \text{ K}] \end{cases} \quad (44)$$

The graphical representation of the energy production and system energy consumption during the mostly sunny week is given in Figure 4.

Figure 4 depicts the global energy production in optimum conditions and measured system energy consumption, with the X-Axis representing the number of experimental days and the Y-Axis representing the energy generation (blue line) and energy consumption (Wh) (red line) during the mostly sunny week. Thus, we observe that, according to the obtained results, the average energy production of the solar tracking device is rated at 10.72 Wh, which compensates for the overall system energy consumption of 7.13 Wh. Additionally, it is visible that the global energy production formula computes the power generation of

the dual-axis solar tracker with a minor relative error rate $err = 0.04$. According to the experimental data from Table 3, which is associated with the partly cloudy week, we can compute the global energy production by using the same premise as stated in the first test scenario.

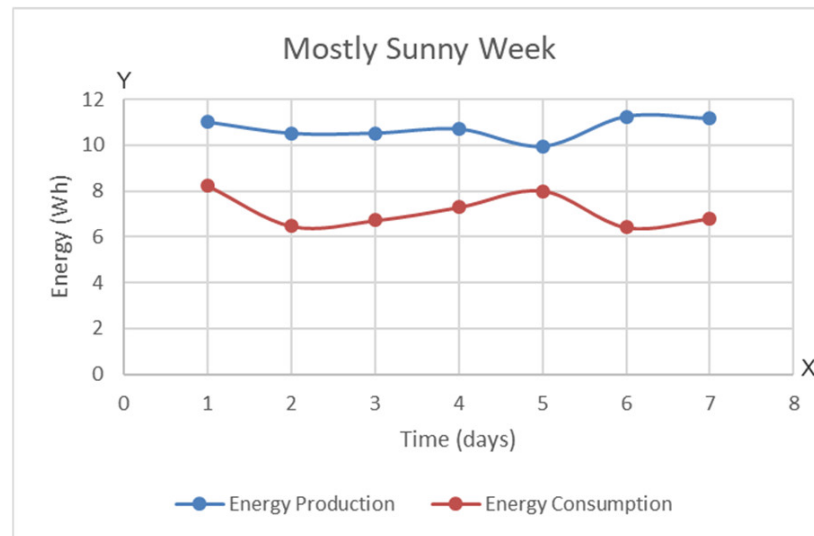


Figure 4. Global Energy Production of the Solar Tracking Device for the Mostly Sunny Week.

Table 3. Experimental results regarding Solar Panel Energy Generation and Storage, as well as System Energy Consumption during the Partly Cloudy Week [21].

Time	Solar Panel Output Voltage (V)	Solar Panel Output Current (A)	Accumulator Input Voltage (V)	Accumulator Charging Current (A)	Accumulator Discharging Current (A)	Solar Panel Power Gain (Wh)	System Energy Consumption (Wh)	UV Index
Day 8	17.15	0.49	12.42	0.45	0.45	5.68	6.58	4
Day 9	17.04	0.47	12.41	0.38	0.36	4.8	5.58	4
Day 10	17.29	0.5	12.36	0.47	0.41	5.85	6.05	3
Day 11	16.66	0.43	12.36	0.45	0.39	5	5.84	3
Day 12	16.62	0.44	12.3	0.4	0.37	4.98	5.55	4
Day 13	16.8	0.5	12.39	0.48	0.37	5.98	5.61	4
Day 14	17	0.54	12.37	0.51	0.5	6.34	7.28	4
Average	16.9371	0.4814	12.3728	0.4485	0.4071	5.5185	6.07	3.7142

Therefore, by substituting all known parameters, we obtained the results, as presented in equation system (45):

$$\begin{cases}
 E_P = A \times \frac{[U - (T - 298)\% \times U] \times I}{S} \times H \times SRF_G \\
 E_{P8} = 1548 \times \frac{[12.42 - (298 - 298)\% \times 12.42] \times 0.45}{1548} \times 1 \times 1 = 5.58 \\
 E_{P9} = 1548 \times \frac{[12.41 - (298 - 298)\% \times 12.41] \times 0.38}{1548} \times 1 \times 1 = 4.71 \\
 E_{P10} = 1548 \times \frac{[12.36 - (298 - 298)\% \times 12.36] \times 0.47}{1548} \times 1 \times 1 = 5.80 \\
 E_{P11} = 1548 \times \frac{[12.36 - (298 - 298)\% \times 12.36] \times 0.45}{1548} \times 1 \times 1 = 5.56 \\
 E_{P12} = 1548 \times \frac{[12.30 - (298 - 298)\% \times 12.30] \times 0.4}{1548} \times 1 \times 1 = 4.92 \\
 E_{P13} = 1548 \times \frac{[12.39 - (298 - 298)\% \times 12.39] \times 0.48}{1548} \times 1 \times 1 = 5.94 \\
 E_{P14} = 1548 \times \frac{[12.37 - (298 - 298)\% \times 12.37] \times 0.51}{1548} \times 1 \times 1 = 6.30 \\
 T \in [298 \text{ K}; 338 \text{ K}]
 \end{cases} \tag{45}$$

The graphical representation of the energy production and system energy consumption during the partly cloudy week is provided in Figure 5.

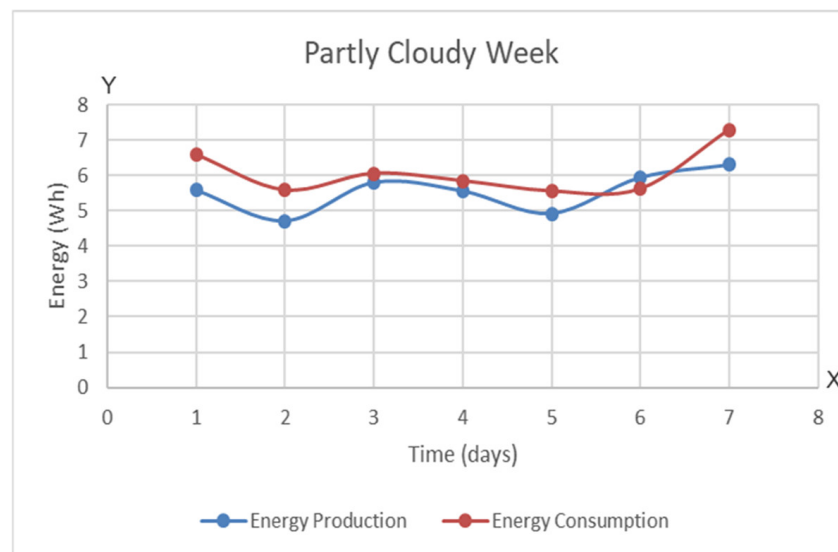


Figure 5. Global Energy Production of the Solar Tracking Device for the Partly Cloudy Week.

Figure 5 presents the global energy production in optimum conditions and measured system energy consumption, with the X-Axis representing the number of experimental days and the Y-Axis representing the power generation (blue line) and energy consumption (Wh) (red line) during the partly cloudy week. The equation system solutions (45) show that the average energy production of the solar tracking device is rated at 5.54 Wh, which is outperformed by the system's energy consumption of 6.07 Wh. It is observable that the relative error rate between the computed E_p and the measured power gain is only $err = 0.03$.

Regarding the second test scenario, we considered the following values for the variables from equation system (14): the total area of the PV panel is equal to the usable PV cell surface ($A = S = 1548 \text{ cm}^2$); the temperature $T = 298 \text{ K}$; the solar radiation level is $H = 1 \text{ kW/m}^2$; the global reliability factor is SRF_G is a variation extracted from equation systems (39) and (41). The measured voltage and current values were extracted from columns 4 and 5 of Tables 2 and 3. Thus, by substituting all variables with their default values, we obtained the global energy production for the mostly sunny week according to equation system (46):

$$\left\{ \begin{array}{l}
 E_p = A \times \frac{[U - (T - 298)\% \times U] \times I}{S} \times H \times SRF_G \\
 E_{p1} = 1548 \times \frac{[12.5 - (298 - 298)\% \times 12.5] \times 0.88}{1548} \times 1 \times 0.73 = 8.03 \\
 E_{p2} = 1548 \times \frac{[12.37 - (298 - 298)\% \times 12.37] \times 0.85}{1548} \times 1 \times 0.72 = 7.56 \\
 E_{p3} = 1548 \times \frac{[12.38 - (298 - 298)\% \times 12.38] \times 0.85}{1548} \times 1 \times 0.73 = 7.67 \\
 E_{p4} = 1548 \times \frac{[12.45 - (298 - 298)\% \times 12.45] \times 0.86}{1548} \times 1 \times 0.75 = 8.02 \\
 E_{p5} = 1548 \times \frac{[12.44 - (298 - 298)\% \times 12.44] \times 0.8}{1548} \times 1 \times 0.76 = 7.56 \\
 E_{p6} = 1548 \times \frac{[12.51 - (298 - 298)\% \times 12.5] \times 0.9}{1548} \times 1 \times 0.73 = 8.21 \\
 E_{p7} = 1548 \times \frac{[12.55 - (298 - 298)\% \times 12.55] \times 0.89}{1548} \times 1 \times 0.75 = 8.37 \\
 T \in [298 \text{ K}; 338 \text{ K}]
 \end{array} \right. \quad (46)$$

The graphical representation of the energy production and system energy consumption during the mostly sunny week is generated in Figure 6.

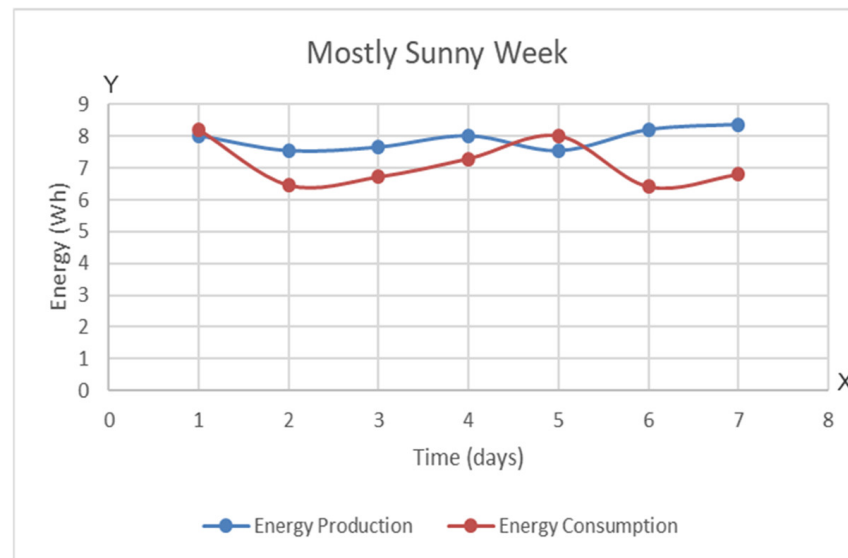


Figure 6. Modified Global Energy Production of the Solar Tracking Device using Reliability-Oriented Metrics for the Mostly Sunny Week.

Figure 6 illustrates the modified global energy production considering 73% availability, with the X-Axis representing the number of experimental days and the Y-Axis representing the power generation (blue line) and energy consumption (Wh) (red line) during the mostly sunny week. The global energy production term is expressed concerning the SRF parameter. Thus, we observe that, according to the obtained results, the average energy production of the solar tracking device is rated at 7.91 Wh, which still compensates for the general system energy consumption of 7.13 Wh. According to the experimental data from Table 3, which is associated with the partly cloudy week, we can compute the global energy production by using the same values as stated in the second test scenario. Therefore, by substituting all known parameters, we obtain the results, as presented in equation system (47):

$$\left\{ \begin{array}{l} E_P = A \times \frac{[U - (T - 298)\% \times U] \times I}{S} \times H \times SRF_G \\ E_{P8} = 1548 \times \frac{[12.42 - (298 - 298)\% \times 12.42] \times 0.45}{1548} \times 0.73 = 4.07 \\ E_{P9} = 1548 \times \frac{[12.41 - (298 - 298)\% \times 12.41] \times 0.38}{1548} \times 0.73 = 3.43 \\ E_{P10} = 1548 \times \frac{[12.36 - (298 - 298)\% \times 12.36] \times 0.47}{1548} \times 0.74 = 4.29 \\ E_{P11} = 1548 \times \frac{[12.36 - (298 - 298)\% \times 12.36] \times 0.45}{1548} \times 0.73 = 4.05 \\ E_{P12} = 1548 \times \frac{[12.30 - (298 - 298)\% \times 12.30] \times 0.4}{1548} \times 0.76 = 3.73 \\ E_{P13} = 1548 \times \frac{[12.39 - (298 - 298)\% \times 12.39] \times 0.48}{1548} \times 0.75 = 4.45 \\ E_{P14} = 1548 \times \frac{[12.37 - (298 - 298)\% \times 12.37] \times 0.51}{1548} \times 0.75 = 4.72 \\ T \in [298 \text{ K}; 338 \text{ K}] \end{array} \right. \quad (47)$$

The graphical representation of the energy production during the partly cloudy week can be observed in Figure 7. The average E_P is now rated at 4.10 Wh, which is considerably lower than the overall energy consumption of the entire system 6.07 Wh, meaning that the entire setup will require additional energy supplies from the power grid when the solar tracker operates under 73% availability conditions.

Figure 7 illustrates the modified global energy production considering 73% availability, with the X-Axis representing the number of experimental days and the Y-Axis representing the power generation (blue line) and energy consumption (Wh) (red line) during the partly cloudy week. At this point, we can analyze the impact of the SRF parameter on the global energy production by generating the solar tracker's power generation over two weeks, as can be seen in Figure 8.

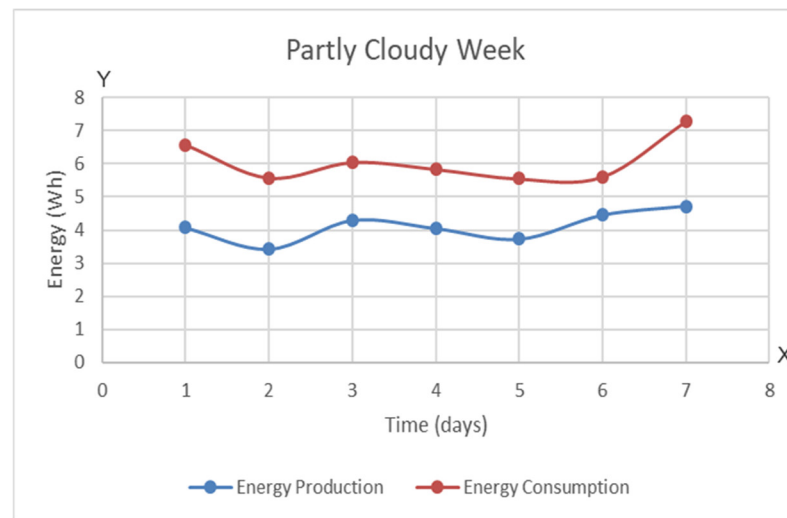


Figure 7. Modified Global Energy Production of the Solar Tracking Device using Reliability-Oriented Metrics for the Partly Cloudy Week.

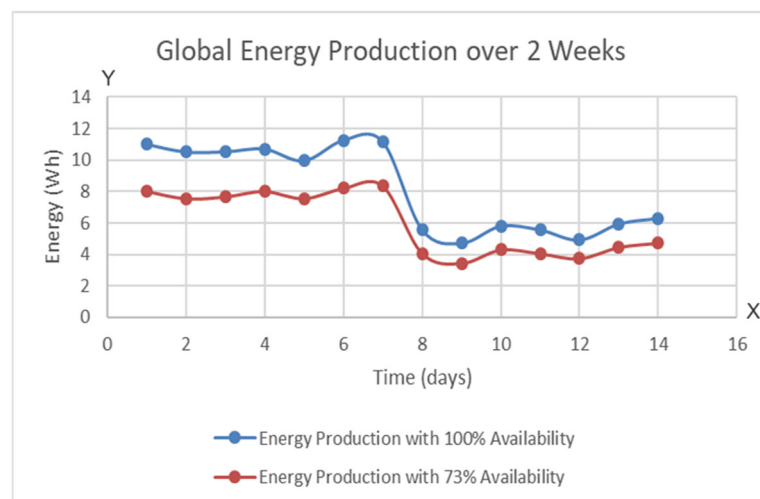


Figure 8. Global Energy Production of the Solar Tracking Device with and without Reliability-Oriented Metrics over Two Weeks.

Figure 8 illustrates the global energy production considering two levels of availability, with the X-Axis representing the number of experimental days and the Y-Axis representing the energy production (Wh) with 100% availability (blue line) and energy generation with 73% availability (Wh) (red line) over two weeks. By concatenating the mostly sunny week together with the partly cloudy week, we observe that the average energy production for both weeks is 8.13 Wh when the dual-axis solar tracker operates without system errors ($SRF_G = 1$), and 6.01 Wh when the solar tracker is affected by mixed system errors (hardware, software, and in-circuit errors), resulting in a significant power generation reduction of 26.11%. The proposed global energy production equation presents several advantages over state-of-the-art formulas [17,18], as follows: (a) it uses only seven parameters for computing the energy production, holding the average position between work [17] which makes use of 14 parameters, and work [18] that utilizes five parameter values; (b) it is tailored towards static and mobile PV systems, in comparison with works [17,18] which can calculate the energy production only for the static model; (c) it employs novel reliability-oriented metrics that classify robust and durable solar tracking systems according to their performance ratio, showing that fault coverage can significantly impact the solar tracker's energy production.

Finally, to demonstrate the validity of the reliability-oriented metrics, a comparison between the proposed *SRF* parameter and the traditional *PR* factor is realized on the two-week experimental dataset, as presented in Figure 9. The global energy production over two weeks was calculated first, using the *SRF* parameter from equation systems (39) and (41), and secondly, by replacing the *PR* factor with its default value of 0.75. According to the statistical data, the global energy production computation using the *PR* factor is around 1.50% less accurate than the modified energy production formula. Nevertheless, we estimate that the gap between the values widens depending on the fault coverage data obtained from the two-week experimental dataset, representing a future research direction.

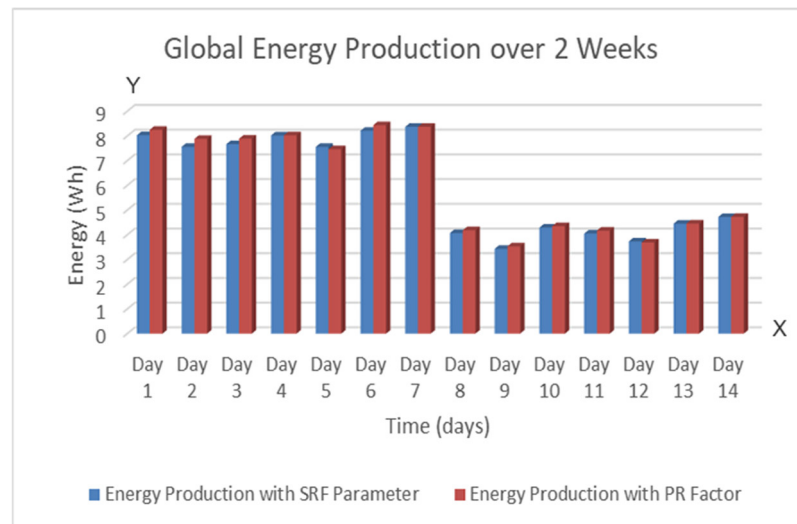


Figure 9. Global Energy Production Computation of the Solar Tracking Device using the *SRF* Parameter (blue bar) and *PR* Factor (red bar).

5. Conclusions

This paper presents a modified global energy production computation formula based on a novel *SRF* parameter that describes the reliability and availability of a dual-axis solar tracker. Additionally, we proposed a self-sufficient energy management design of a solar-powered smart home automation system that integrates a hybrid testing platform for determining the fault coverage of the solar tracker, as well as a Cloud platform for monitoring and storing data from the PV panel. By applying the *SRF* in the global energy production formula of solar tracking systems, we can predict with a minimal error rate of 0.03–0.04 the energy generation in real time, allowing proper energy management of the entire smart home automation system. Experimental results show that the energy production computation constantly fluctuates over several days due to the *SRF* parameter variation, showing a 26.11% reduction when the dual-axis solar tracker’s availability is affected by system errors and maximum power generation when the solar tracking device is operating in optimal conditions.

To demonstrate the validity of the reliability-oriented metrics, a comparison between the proposed *SRF* parameter and the standard *PR* factor is performed on a two-week experimental dataset, showing a 1.50% accuracy decrease for the *PR* factor in favor of the modified global energy production formula. Therefore, our research indicates that energy production computation is far more complex in solar tracking systems due to software, hardware, and in-circuit errors which affect the system’s stability, resulting in significant energy loss. Therefore, this paper encourages the deployment of low-cost and energy-efficient testing facilities that aid modern solar trackers in monitoring and detecting system errors, ultimately impacting the availability of mobile PV systems.

Author Contributions: Conceptualization, S.L.J., R.R. and R.S.; methodology, S.L.J., R.R. and R.S.; software, S.L.J.; validation, S.L.J., R.R. and M.V.; formal analysis, S.L.J. and R.R.; investigation, S.L.J., R.R. and F.O.; resources, S.L.J., R.S. and R.R.; data curation, S.L.J., R.R. and F.O.; writing—original draft preparation, S.L.J., R.S. and R.R.; writing—review and editing, all authors.; supervision, M.V. All authors have read and agreed to the published version of the manuscript.

Funding: This research received no external funding.

Institutional Review Board Statement: Not applicable.

Informed Consent Statement: Not applicable.

Data Availability Statement: Not applicable.

Conflicts of Interest: The authors declare no conflict of interest.

References

1. Khanna, A.; Kaur, S. Internet of Things (IoT), Applications and Challenges: A Comprehensive Review. *Wirel. Pers. Commun.* **2020**, *114*, 1687–1762. [CrossRef]
2. Forecast End-User Spending on IoT Solutions Worldwide from 2017 to 2025. Available online: <https://www.statista.com/statistics/976313/global-iot-market-size/> (accessed on 27 April 2021).
3. Kim, W.; Jung, I. Smart Sensing Period for Efficient Energy Consumption in IoT Network. *Sensors* **2019**, *19*, 4915. [CrossRef] [PubMed]
4. The Climate Vulnerable Forum Vision. Available online: <https://thecvf.org/marrakech-vision/> (accessed on 27 April 2021).
5. Bouguerra, S.; Yaiche, M.R.; Sangwongwanich, A.; Blaabjerg, F.; Liivik, E. Reliability Analysis and Energy Yield of String-Inverter Considering Monofacial and Bifacial Photovoltaic Panels. In Proceedings of the 2020 IEEE 11th International Symposium on Power Electronics for Distributed Generation Systems (PEDG), Dubrovnik, Croatia, 28 September–1 October 2020; pp. 199–204. [CrossRef]
6. Bostan, V.; Tudorache, T.; Colt, G. Improvement of solar radiation absorption of a PV panel using a Plane low concentration system. In Proceedings of the 2017 10th International Symposium on Advanced Topics in Electrical Engineering (ATEE), Bucharest, Romania, 23–25 March 2017; pp. 778–781. [CrossRef]
7. Ghiani, E.; Pilo, F.; Cossu, S. On the performance ratio of photovoltaic installations. In Proceedings of the 2013 IEEE Grenoble Conference, Grenoble, France, 16–20 June 2013; pp. 1–6. [CrossRef]
8. Jurj, S.L.; Rotar, R.; Opritoiu, F.; Vladutiu, M. Improving the Solar Reliability Factor of a Dual-Axis Solar Tracking System Using Energy-Efficient Testing Solutions. *Energies* **2021**, *14*, 2009. [CrossRef]
9. Amit, S.; Koshy, A.S.; Sampriya, S.; Joshi, S.; Ranjitha, N. Internet of Things (IoT) enabled Sustainable Home Automation along with Security using Solar Energy. In Proceedings of the 2019 International Conference on Communication and Electronics Systems (ICES), Coimbatore, India, 17–19 July 2019; pp. 1026–1029. [CrossRef]
10. Singh, M.K.; Sajwan, S.; Pal, N.S. Solar assisted advance smart home automation. In Proceedings of the 2017 International Conference on Information, Communication, Instrumentation and Control (ICICIC), Indore, India, 17–19 August 2017; pp. 1–6. [CrossRef]
11. Asham, A.D.; Hanaa, M.; Alyoubi, B.; Badawood, A.M.; Alharbi, I. A simple integrated smart green home design. In Proceedings of the 2017 Intelligent Systems Conference (IntelliSys), London, UK, 7–8 September 2017; pp. 194–197. [CrossRef]
12. Shahin, F.B.; Tawheed, P.; Haque, M.F.; Hasan, M.R.; Khan, M.N.R. Smart home solutions with sun tracking solar panel. In Proceedings of the 2017 4th International Conference on Advances in Electrical Engineering (ICAEE), Dhaka, Bangladesh, 28–30 September 2017; pp. 766–769. [CrossRef]
13. Cabras, M.; Pilloni, V.; Atzori, L. A novel Smart Home Energy Management system: Cooperative neighbourhood and adaptive renewable energy usage. In Proceedings of the 2015 IEEE International Conference on Communications (ICC), London, UK, 8–12 June 2015; pp. 716–721. [CrossRef]
14. Elkazaz, M.; Sumner, M.; Davies, R.; Pholboon, S.; Thomas, D. Optimization based Real-Time Home Energy Management in the Presence of Renewable Energy and Battery Energy Storage. In Proceedings of the 2019 International Conference on Smart Energy Systems and Technologies (SEST), Porto, Portugal, 9–11 September 2019; pp. 1–6. [CrossRef]
15. Soltowski, B.; Strachan, S.; Anaya-Lara, O.; Frame, D.; Dolan, M. Using smart power management control to maximize energy utilization and reliability within a microgrid of interconnected solar home systems. In Proceedings of the 2017 IEEE Global Humanitarian Technology Conference (GHTC), San Jose, CA, USA, 19–22 October 2017; pp. 1–5. [CrossRef]
16. Rotar, R.; Jurj, S.L.; Opritoiu, F.; Vladutiu, M. Fault Coverage-Aware Metrics for Evaluating the Reliability Factor of Solar Tracking Systems. *Energies* **2021**, *14*, 1074. [CrossRef]
17. Aste, N.; del Pero, C.; Leonforte, F.; Manfren, M. A simplified model for the estimation of energy production of PV systems. *Energy* **2013**, *59*, 503–512. [CrossRef]
18. Diantari, R.A.; Pujotomo, I. Calculation of electrical energy with solar power plant design. In Proceedings of the 2016 International Seminar on Intelligent Technology and Its Applications (ISITIA), Lombok, Indonesia, 28–30 July 2016; pp. 443–446. [CrossRef]

19. Jurj, S.L.; Rotar, R.; Opritoiu, F.; Vladutiu, M. Efficient Implementation of a Self-Sufficient Solar-Powered Real-Time Deep Learning-Based System. In *Proceedings of the 21st EANN (Engineering Applications of Neural Networks) 2020 Conference*; Iliadis, L., Angelov, P., Jayne, C., Pimenidis, E., Eds.; Springer: Cham, Switzerland, 2020; Volume 2, pp. 99–118. [[CrossRef](#)]
20. Susany, R.; Rotar, R. Remote Control Android-Based Applications for a Home Automation Implemented with Arduino Mega 2560 and ESP 32. *Tech. Romanian J. Appl. Sci. Technol.* **2020**, *2*, 1–8. [[CrossRef](#)]
21. Jurj, S.L.; Rotar, R.; Opritoiu, F.; Vladutiu, M. Hybrid testing of a solar tracking equipment using in-circuit testing and JTAG debugging strategies. In *Proceedings of the 2021 IEEE International Conference on Environment and Electrical Engineering and 2020 IEEE Industrial and Commercial Power Systems Europe (EEEIC/I&CPS Europe)*, Bari, Italy, 7–10 September 2021.